Journal of ELECTRONIC MATERIALS, Vol. 45, No. 3, 2016
DOI: 10.1007/s11664-015-4089-6

Effects of Lattice Defects and Niobium Doping on Thermoelectric Properties of Calcium Manganate Compounds for Energy Harvesting Applications

AYELET GRAFF[1] and YARON AMOUYAL[1,2]

1.—Department of Materials Science and Engineering, Technion - Israel Institute of Technology, 32000 Haifa, Israel. 2.—e-mail: amouyal@tx.technion.ac.il

We have investigated the thermoelectric (TE) properties of Ruddlesden–Popper (RP) $CaO(CaMnO_3)_m$ *n*-type compounds, to be applied for TE waste heat recovery at elevated temperatures. We prepared several Nb-doped and undoped $CaO(CaMnO_3)_m$ compounds having different CaO planar densities by controlling the Ca content via solid-state reaction, and characterized the resulting microstructures by x-ray diffraction analysis and high-resolution scanning electron microscopy. The thermal conductivity, electrical conductivity, and TE thermopower of the different compounds were measured in the range from 300 K through 1000 K. We observed a remarkable reduction in thermal conductivity as a result of increasing the CaO planar density for the Nb-doped RP compounds, from a value of 2.9 W m^{-1} K^{-1} for $m = \infty$ down to 1.3 W m^{-1} K^{-1} for $m = 1$ at 1000 K. This trend was, however, accompanied by a corresponding reduction in electrical conductivity from 76 Ω^{-1} cm^{-1} to 2.9 Ω^{-1} cm^{-1}, which is associated with electron scattering. Finally, we propose an approach that enables optimization of the TE performance of these RP compounds.

Key words: Thermoelectric materials, thermal conductivity, calcium manganates, phonon scattering, microstructure–property relationship

INTRODUCTION

One of the directions in the search for alternative energy sources is to capture waste heat and convert it into electricity using thermoelectric (TE) generators. Such generators are based on the Seebeck effect, in which a temperature (T) gradient prevailing within a material initiates diffusion of charge carriers along this gradient, thus creating an open-circuit voltage (V) between the hot and cold poles.[1,2] The temperature-dependent Seebeck coefficient, $S(T)$, which is commonly referred to as the *thermopower*, is accordingly defined as follows:

$$S(T) \equiv \frac{\partial V}{\partial T}. \tag{1}$$

A TE generator commonly consists of an array of TE couples comprising *n*- and *p*-type legs, which are connected electrically in series and thermally in parallel. Such generators are solid-state devices having no moving parts, being noiseless, vibrationless, environmentally friendly, and extremely durable.[3,4] An efficient TE material is characterized by a high TE *figure of merit*, ZT, which is defined as

$$ZT \equiv \frac{S^2 \sigma T}{\kappa}, \tag{2}$$

where σ and κ are the material's electrical and thermal conductivities, respectively. High heat-to-electrical power conversion efficiency requires high ZT values, which can be obtained by either large Seebeck coefficient, high electrical conductivity, or

(Received June 1, 2015; accepted September 23, 2015; published online October 14, 2015)

low thermal conductivity.[1] The latter is, essentially, a sum of two contributions: $\kappa = \kappa_p + \kappa_e$, where κ_p is related to phonon vibrations and κ_e is related to charge carrier conduction.[5] Since all three of the physical magnitudes embodied in ZT depend on the carrier concentration, improving ZT by minimizing the thermal conductivity without significantly affecting the electrical conductivity remains one of the great challenges in the study of TE materials.

One of today's attractive classes of TE materials are oxides. They offer several key advantages, including structural and chemical stability at high temperatures, nontoxicity, and low cost.[6–9] The major shortcoming of TE oxides is, however, their relatively low ZT values. Whereas the figures of merit of both Na_xCoO_2[10] and $Ca_3Co_4O_9$[11] p-type cobaltates approach unity at 1000 K, the ZT values of other n-type oxides are significantly lower ($\sim$0.3 at 1000 K) and should thus be improved.[6,9,12] Since TE properties are highly sensitive to the finest features of the microstructure, one of the most promising approaches to enhance TE performance is to reduce κ, with little or no effect on σ. This can be achieved by designing layered materials or superlattices,[13–16] where the key feature in reducing κ is the large number of interfaces per unit volume, thereby initiating phonon scattering.

The present study focuses on $CaO(CaMnO_3)_m$ n-type compounds consisting of modulated m perovskite $CaMnO_3$ layers separated by single rock-salt CaO layers, which belong to the Ruddlesden–Popper (RP) class of compounds; the latter exhibit intriguing physical properties, such as optical, ferroelectric, piezoelectric, magnetic, catalytic, and thermoelectric effects.[17–22] We previously reported on significant reduction of thermal conductivity in these compounds due to additions of extra CaO planar defects.[23] Herein, we aim to draw a correlation between the overall TE properties, namely the Seebeck coefficient and the electrical and thermal conductivities, of pure and niobium-doped CaO $(CaMnO_3)_m$ compounds and the periodicity of the planar CaO defects, denoted by the m value. We are, additionally, interested in studying the effects of Nb doping on the TE properties, and how they vary with the m value.

EXPERIMENTAL PROCEDURES

Two groups of compounds, namely CaO $(CaMnO_3)_m$ with m = 1, 2, 3, and ∞ and CaO $(CaMn_{1-x}Nb_xO_3)_m$ with x = 0.04 and m = 1, 2, 3, 4, 5, and ∞, were synthesized from pure oxide powders mixed in the appropriate stoichiometric ratios. The two main raw oxide powders used for preparation of the undoped compounds were calcium carbonate ($CaCO_3$) powder with ca. 14 μm average particle size (Merck) and manganese dioxide (MnO_2) with ca. 50 μm average particle size (Baker Co.). The major impurities present in the raw powders, as declared by the manufacturers, were SO_4 (<0.03%), Mg (<0.02%), Na (<0.2%), and Sr (<0.1%) for $CaCO_3$ and Cl (<0.01%), NO_3 (<0.05%), SO_4 (<0.05%), and Fe (<0.03%) for MnO_2. The Nb-doped compounds were prepared by mixing Nb_2O_5 pure powder with the above $CaCO_3$ and MnO_2 raw powders in the appropriate ratios to obtain a doping level of x = 4 at.%. This doping level is conventional for $CaMnO_3$-based compounds;[24–28] moreover, it lies within the concentration range of 2 at.% to 5 at.% Nb, reported to yield improved ZT values for specific Nb-doped systems.[28] Both classes of compounds were prepared using a standard solid-state reaction protocol,[20] which includes mixing of the powders and ball-milling for 24 h, resulting in ca. 2 μm grain size, followed by room-temperature uniaxial pressing under pressure of 900 MPa to form both pellet- (12.5 mm diameter × ca. 2 mm thick) and bar-shaped (2 mm × 2 mm × 12.5 mm) specimens. Then, the specimens were sintered in air in several stages with increasing temperature ranging from 1223 K up to 1673 K, which are optimized for each compound, for 24 h in each step. The process was determined by sintering at a given temperature and regrinding to fine powder, followed by x-ray diffraction (XRD) analysis using a Siemens D5000 powder diffractometer with angular resolution of 0.02°, to ensure that the desirable single-phase RP compounds were obtained. This process was repeated at the following temperatures with intermediate grinding steps: 1223 K, 1373 K, 1473 K, 1573 K, 1623 K, and 1673 K until the desired material was obtained. Finally, all sintered pellet- or bar-shaped specimens were air-cooled.[23]

Microstructure characterization of the samples was carried out using a Zeiss Ultra Plus high-resolution scanning electron microscope (HRSEM), equipped with a Schottky field-emission electron gun. The images presented were taken using a secondary-electron detector operated at 4 keV.

The temperature-dependent electrical conductivity, $\sigma(T)$, and thermopower, $S(T)$, were measured in the temperature range from 300 K through 1000 K using a Nemesis SBA-458 apparatus (Netzsch GmbH, Selb, Germany), which is designed for simultaneous measurements of electrical conductivity and thermopower for planar geometry.[29,30]

We determined the materials' thermal conductivity, κ, by measuring their temperature-dependent thermal diffusivity, $\alpha(T)$, and specific heat, $C_p(T)$, as well as the density, ρ; κ was then calculated as[1]

$$\kappa(T) = \alpha(T) \cdot \rho \cdot C_p(T). \quad (3)$$

We employed a Microprobe LFA-457 laser flash analyzer (LFA; Netzsch GmbH, Selb, Germany) to directly measure the thermal diffusivity of pellet-shaped specimens for the temperature range from 300 K through 1000 K, with instrumental accuracy of 2%. The material densities were measured at room temperature (Table I), and the dependence on

temperature was neglected. The temperature-dependent heat capacity was measured simultaneously in the LFA using a comparative method with a pure Al_2O_3 reference sample of similar geometry. The resulting accuracy of the evaluation of thermal conductivity values is 10%.

RESULTS

Figure 1 displays HRSEM micrographs of the (a) undoped and (b) Nb-doped $m = \infty$ specimens. The XRD patterns acquired from these specimens are shown in Fig. 1c and d, respectively. The XRD data confirm that all compounds exhibit the expected single-phase states. The periodicities of $m = 1$ through 3 possess a tetragonal crystal structure with *I4/mmm* space group symmetry, and the $m = \infty$ specimen possesses an orthorhombic crystal structure with *Pnma* space group symmetry. We note that the $m = 1$ structure is commonly reported to possess *I41/acd* space group symmetry, in several experimental and computational studies.[31–35] This, however, has no practical meaning for the interpretation of the results of this study in terms of the TE perfor-

Table I. Room-temperature values of specimen bulk density (g cm^{-3}) and relative density (%), as measured for undoped ($m = \infty$, 1, 2, and 3) and Nb-doped ($m = \infty$, 1, 2, 3, 4*, and 5*) compounds

m-Value	Undoped (g cm^{-3})	Undoped (%)	Nb-Doped (g cm^{-3})	Nb-Doped (%)
$m = \infty$	3.53 ± 0.04	79.0 ± 0.9	3.94 ± 0.04	88.2 ± 0.9
$m = 1$	3.08 ± 0.01	75.8 ± 0.3	3.13 ± 0.04	77.0 ± 1.0
$m = 2$	3.47 ± 0.02	81.7 ± 0.5	3.27 ± 0.05	77.0 ± 1.2
$m = 3$	3.14 ± 0.01	73.0 ± 2.1	3.13 ± 0.09	72.7 ± 2.1
$m = 4^*$	–	–	3.59 ± 0.01	–
$m = 5^*$	–	–	3.62 ± 0.01	–

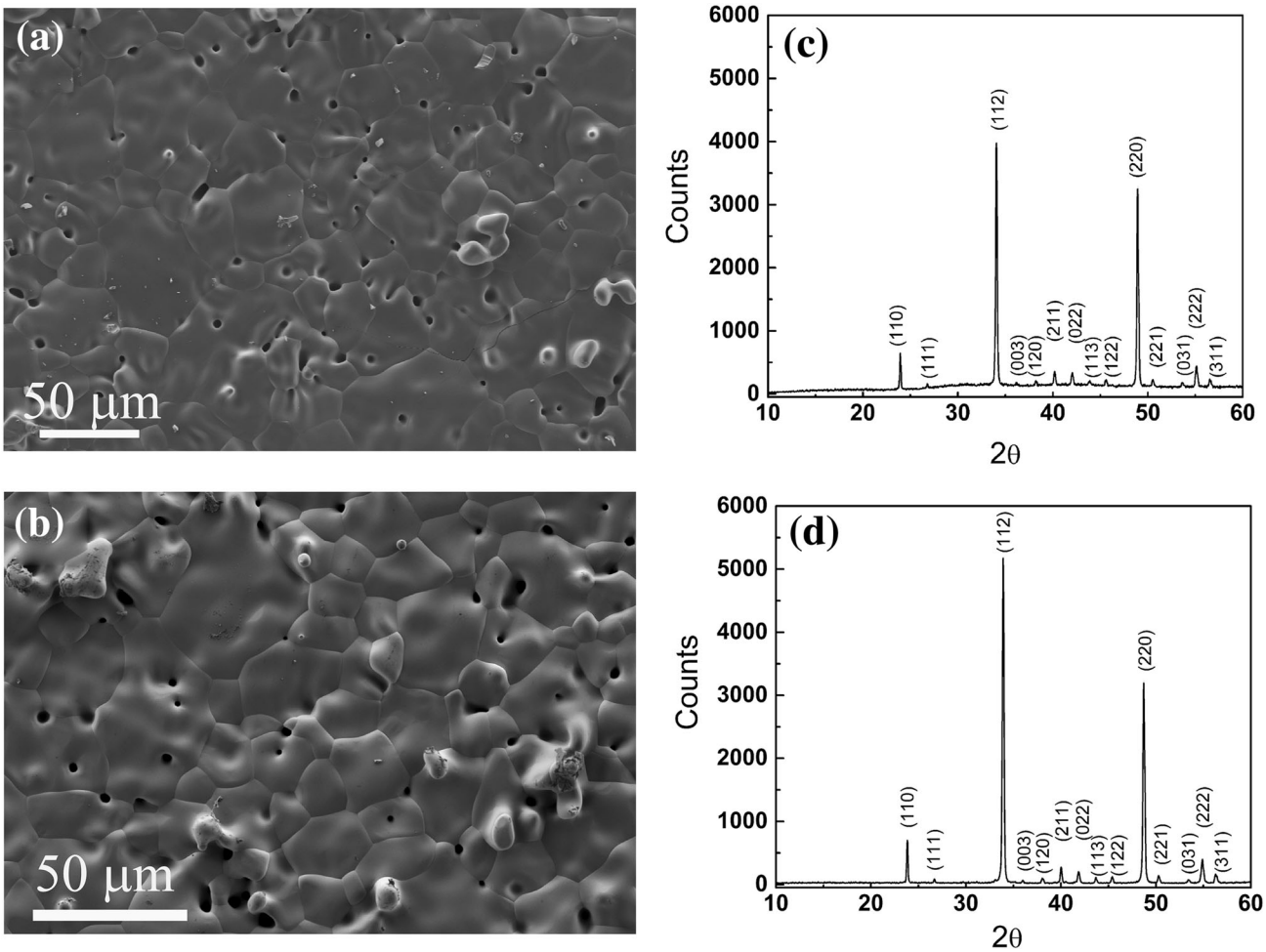

Fig. 1. High-resolution scanning electron microscope (HRSEM) images acquired from the undoped (a) and the Nb-doped (b) compounds with $m = \infty$ periodicity, and their corresponding XRD patterns (c) and (d), respectively.

mance, since both the *I4/mmm* and *I41/acd* space group symmetries differ by only distortions and rotations of the oxide polyhedra, which is not detectable by XRD; the same CaO layering exists for both symmetries. Further details of the analyzed crystal structure appear elsewhere.[23] The XRD patterns collected from the $m = 4$ and $m = 5$ compounds do not fit any of the above *I4/mmm* space groups; they rather correspond with a combination of the following two phases: $m = \infty$ and $m = 3$; therefore, they are marked as $m = 4^*$ and $m = 5^*$ hereinafter. Comparison between both the HRSEM micrographs and XRD patterns in Fig. 1 indicates that doping does not lead to any change in the microstructure in terms of either grain size (Fig. 1a and b) or formation of new phases (Fig. 1c and d). The former conclusion is based on grain size measurements applying the intersecting line method, yielding average values of 17.40 ± 0.40 μm and 17.60 ± 0.45 μm for the undoped and Nb-doped $m = \infty$ compounds, respectively. In addition, no presence of sub-micrometer-size second-phase precipitates is detectable in either the XRD or HRSEM data.

Since we are interested in the effects of both lattice periodicity (m value) and Nb doping on the TE properties, we plot the temperature dependence of each of the TE properties for different m values, with and without doping. Figure 2 shows the temperature dependence of the thermal conductivity for different m values, with and without doping. These

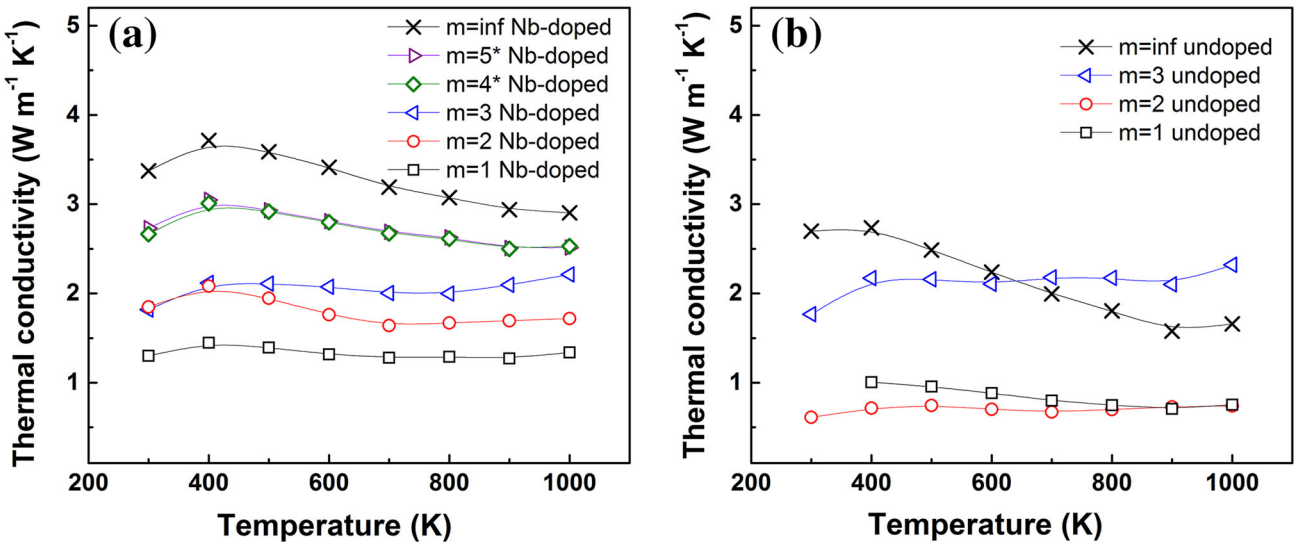

Fig. 2. (Color online) Temperature-dependent thermal conductivity measured for the (a) Nb-doped and (b) undoped compounds with different periodicities of $m = \infty$ (inf., cross markers), $m = 1$ (black squares), $m = 2$ (red circles), $m = 3$ (blue left-triangles), $m = 4^*$ (green diamonds), and $m = 5^*$ (purple right-triangles).

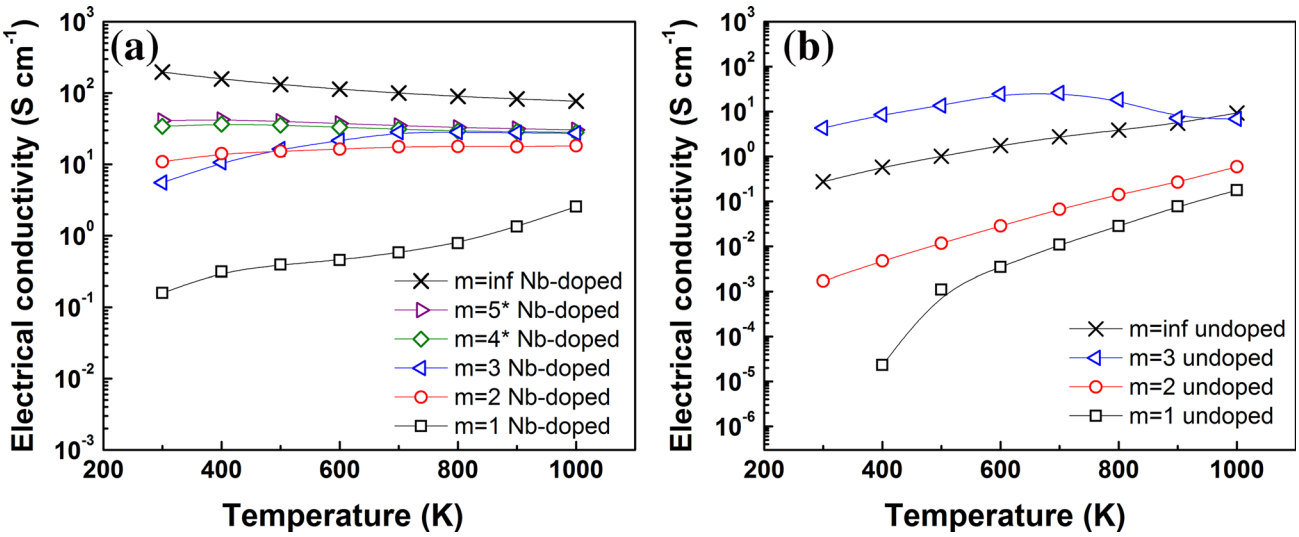

Fig. 3. (Color online) Temperature-dependent electrical conductivity measured for the (a) Nb-doped and (b) undoped compounds with different periodicities of $m = \infty$ (inf., cross markers), $m = 1$ (black squares), $m = 2$ (red circles), $m = 3$ (blue left-triangles), $m = 4^*$ (green diamonds), and $m = 5^*$ (purple right-triangles).

values were evaluated based on Eq. 3, employing the thermal diffusivity values that were measured directly, and the measured bulk density values appearing in Table I.

For the Nb-doped samples, a remarkable reduction of thermal conductivity due to introduction of CaO planes can be observed, e.g., from a value of 2.9 W m^{-1} K^{-1} for $m = \infty$ down to 1.3 W m^{-1} K^{-1} for $m = 1$ at 1000 K. It is noteworthy that the thermal conductivity decreases systematically with increasing CaO planar density (decreasing m value). We highlight that these differences in thermal conductivity values cannot be attributed to the differences in the specimens' bulk densities, as appear in Table I, but to the m values only. Additionally, the differences in thermal conductivity of all RP variants do not change significantly with temperature, and do not converge at high temperatures. Interestingly, the Nb-doped samples (Fig. 2a) exhibit thermal conductivity values that are larger by ca. 0.5 W m^{-1} K^{-1} to 1 W m^{-1} K^{-1} than those of the undoped samples (Fig. 2b), probably due to the electronic contribution to the thermal conductivity. It is also noteworthy that the systematic behavior of the thermal conductivity dependence on the m value distinguished for the Nb-doped compounds (Fig. 2a) is not observed for the undoped compounds (Fig. 2b). This might be associated to possible effects of the Nb dopant on the stacking or ordering of the CaO layers, e.g., lowering their interfacial free energies. Such a tendency for formation of disordered stacking faults or twin boundaries, which might be attributed to local variation of oxygen concentration, has been reported elsewhere.[36] We believe that Nb doping induces similar effects.

The temperature-dependent electrical conductivity values measured for the doped and undoped compounds with different m values are displayed in Fig. 3a and b, respectively. Generally, it is indicated that the electrical conductivity values of all the Nb-doped RP phases (m = 1 through 5) are lower than those of the $m = \infty$ specimen; e.g., the electrical conductivity decreases from a value of 76 Ω^{-1} cm^{-1} for $m = \infty$ to 2.9 Ω^{-1} cm^{-1} for $m = 1$ at 1000 K. This behavior can be associated to the planar density of the insulating rock-salt CaO layers in the polycrystalline RP samples, reducing the electron mean free path. Interestingly, the electrical conductivity for the different m values spans several orders of magnitude, whereas the corresponding variation of thermal conductivity (Fig. 2a) is tens of percent. Moreover, it can be seen that the electrical conductivity values decrease systematically with increasing CaO planar density (decreasing m value). In addition, one can observe that the differences between the electrical conductivity values of the RP phases diminish with increasing temperature, in contrast to the behavior observed for the thermal conductivity values (Fig. 2). It is also indicated that the Nb-doped samples exhibit significantly higher electrical conductivity values than those of the undoped samples, by ca. 2 to 4 orders of magnitude at room temperature, as expected. Among the undoped samples, the electrical conductivity values measured for the $m = \infty$ sample deviate from the expected trend, i.e., $\sigma(m = \infty) > \sigma(m = 3) > \sigma\ (m = 2) > \sigma(m = 1)$, being clearly observed for the Nb-doped samples (Fig. 3a). This might be elucidated in view of the different crystal symmetry of the $m = \infty$ phase with respect to the other RP variants.[23] Alternatively, this trend can be considered as an unexpectedly high conductivity of the m = 3 compound, originating from an uncontrolled level of impurities. The latter are mostly pronounced for the undoped compounds, being negligible for their Nb-doped counterparts.

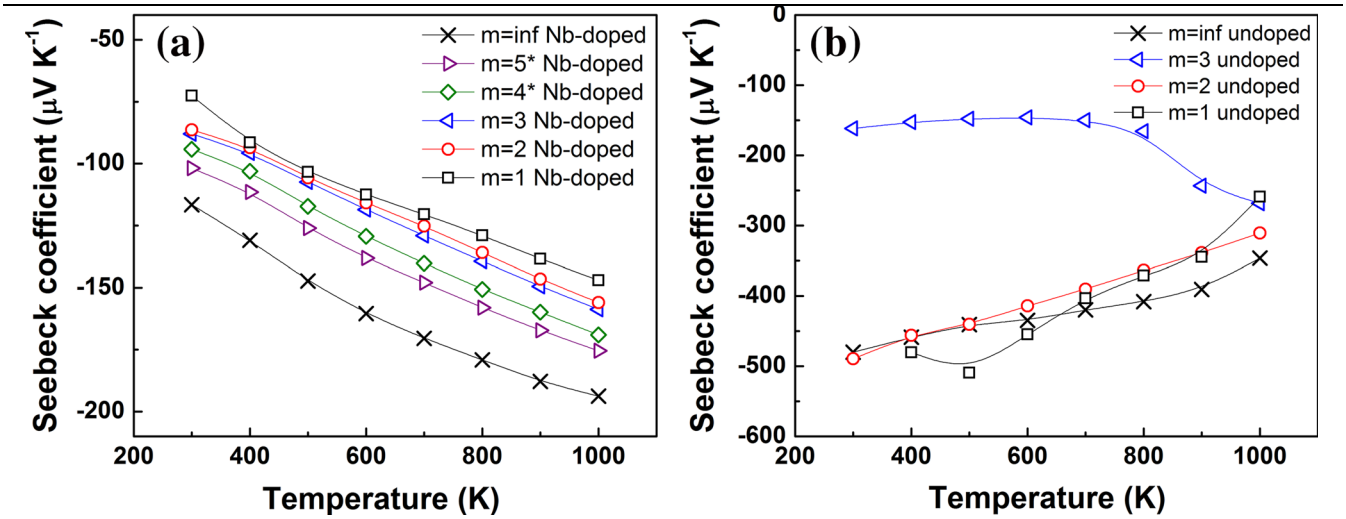

Fig. 4. (Color online) Temperature-dependent Seebeck coefficient (thermopower) measured for the (a) Nb-doped and (b) undoped compounds with different periodicities of $m = \infty$ (inf., cross markers), m = 1 (black squares), m = 2 (red circles), m = 3 (blue left-triangles), $m = 4^*$ (green diamonds), and $m = 5^*$ (purple right-triangles).

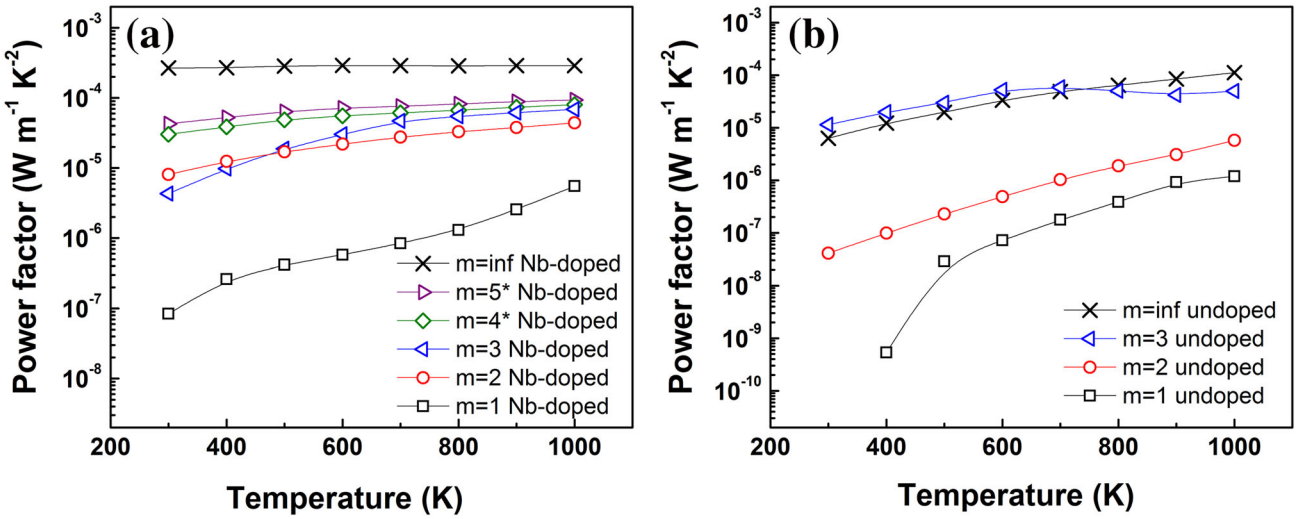

Fig. 5. (Color online) Temperature-dependent power factor (PF) values calculated for the (a) Nb-doped and (b) undoped compounds with different periodicities of $m = \infty$ (inf., cross markers), $m = 1$ (black squares), $m = 2$ (red circles), $m = 3$ (blue left-triangles), $m = 4^*$ (green diamonds), and $m = 5^*$ (purple right-triangles).

The temperature dependence of the thermopower for different m values with and without doping is presented in Fig. 4a and b, respectively. It can be observed that the $|S|$ values of the Nb-doped RP phases (m = 1 through 5) are lower than that of the $m = \infty$ specimen. Additionally, the Nb-doped samples' thermopower values correspond with the CaO planar density as follows: $|S|(m=\infty) > |S|(m=5) > |S|$ $(m = 4) > |S|(m=3) > |S|(m=2) > |S|(m=1)$; this trend is similar to that shown by the electrical conductivity (Fig. 3a). It can be inferred from comparison between Fig. 4a and b that Nb doping reduces the thermopower absolute values, as expected. The nonsystematic behavior shown for the undoped compounds (Fig. 4b) again implies high sensitivity of the thermopower to impurities.

DISCUSSION

Electrical Behavior and Power Factor Calculation

The positive effects of the lattice periodicity, as manifested by the m value, in reducing the thermal conductivity are evident. This behavior has been thoroughly discussed and modeled elsewhere.[23] Notwithstanding these effects, the electrical conductivity is also reduced by these extra CaO planes. There is also an influence of m on the thermopower, as shown in Fig. 4. Whereas the effects of the extra CaO planes on the electrical conductivity can be reasonably elucidated in terms of a reduction of the electron mean free path or electron scattering, their effects on the thermopower may not be elucidated in a straightforward manner. This is because, on the one hand, the average concentration of Nb atoms is identical for all the Nb-doped compounds with different m values in Fig. 4a; on the other hand, the thermopower is mostly determined by the dopant concentrations rather than the defect distribution.[1] In particular, the absolute value of the thermopower decreases with increasing doping levels.[1] To address this behavior, we note that the CaO layers are insulating while the perovskite interlayers are semiconducting. Also, Nb atoms preferentially substitute at Mn sublattice sites,[37] residing in the perovskite substructure. It turns out that the *effective concentration* of Nb dopants, which is defined as their concentration in the semiconducting medium only, becomes larger for decreasing m value, for constant nominal concentration of Nb. This explains the following systematic trend shown in Fig. 4a: $|S|$ $(m=\infty) > |S|(m=5) > |S|(m=4) > |S|(m=3) >$ $|S|$ $(m=2) > |S|(m=1)$.

Interestingly, this mechanism may also be relevant for the trend shown for the electrical conductivity values in Fig. 3a, in which the temperature dependence of $\sigma(T)$ is dictated by the m value. It is shown that $\sigma(T)$ decreases with temperature for $m = \infty$, that is, $\frac{d\sigma}{dT} < 0$ for the entire temperature range, which is typical for metal-like behavior.[38] Conversely, $\sigma(T)$ increases with temperature for m = 1, that is, $\frac{d\sigma}{dT} > 0$ for the entire temperature range, which represents a semiconducting behavior originating from thermal activation of charge carriers.[38] The m = 2 through $m = 5^*$ states exhibit intermediate trends. Following the above-suggested mechanism, we postulate that Nb doping of the m = 1 structure results in an *effective concentration* of Nb dopants that is greater than when doping the $m = \infty$ structure, for a constant value of nominal Nb concentration. In other words, the m = 1 structure is, *effectively*, more heavily doped than its $m = \infty$ counterpart. This is the reason for the semiconducting versus metallic behavior observed for the two structures, respectively. This trend might be

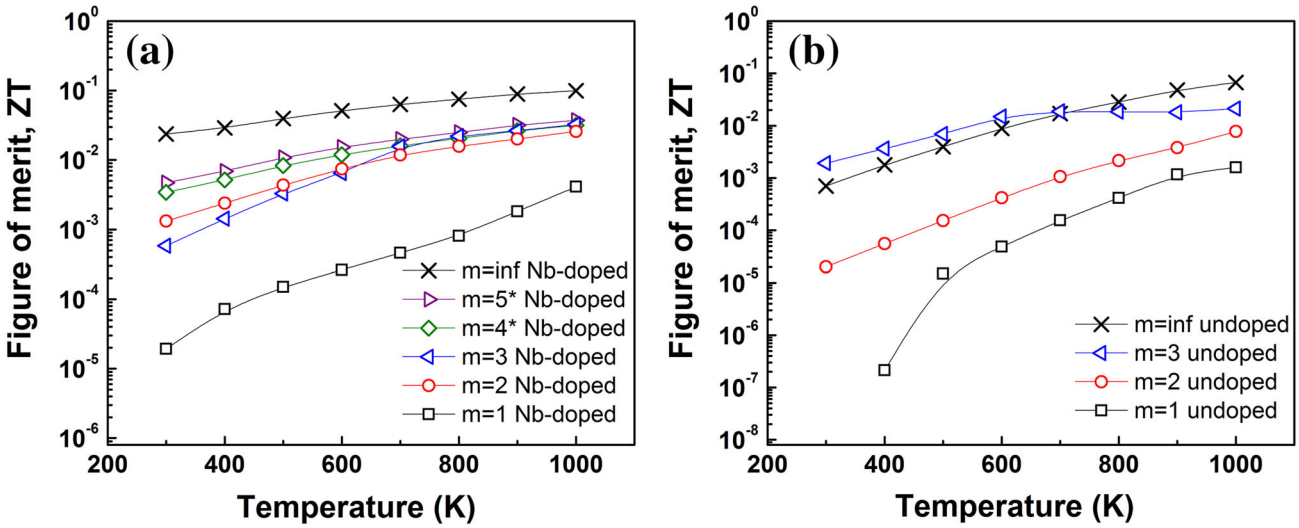

Fig. 6. (Color online) Temperature-dependent figure of merit, *ZT*, calculated for the (a) Nb-doped and (b) undoped compounds with different periodicities of $m = \infty$ (inf., cross markers), $m = 1$ (black squares), $m = 2$ (red circles), $m = 3$ (blue left-triangles), $m = 4^*$ (green diamonds), and $m = 5^*$ (purple right-triangles)..

corroborated by the results reported by Bocher et al. in their thorough study of Nb-doped $CaMnO_3$ ($m = \infty$).[28] They measured the temperature-dependent electrical resistivity values for 2 at.%, 5 at.%, and 8 at.% Nb-doped compounds in the range from 300 K through 1070 K. They showed that the electrical resistivity values increase with temperature for all three compositions, but the rate of increase is the largest for 2 at.% Nb and smallest for 8 at.% Nb. This implies that Nb addition enhances the semiconducting nature of the compound, which corresponds with the above-suggested mechanism.

We note that the electrical conductivity values obtained in this study for the $m = \infty$ structure, ca. 1 S cm^{-1} and 100 S cm^{-1} on average, for the undoped and Nb-doped compounds, respectively, are in the same order of magnitude and slightly larger than those reported by Melo Jorge et al.[39] The latter reported resistivity values of 5 Ω cm and 0.2 Ω cm on average for undoped and 5 at.% Ce-doped $CaMnO_3$, respectively. The above-average values obtained in this study are similar to those reported by Bocher et al., as well.[28] The differences can be associated to the different relative densities obtained by us (Table I) and by those authors. It is also noteworthy that the dependence of the electrical conductivity on temperature exhibits a change of slope for both the undoped and Nb-doped $m = 3$ compounds (Fig. 3). This trend is most pronounced for the Nb-doped compound, where $\sigma(m = 3) < \sigma(m = 2)$ below 500 K and $\sigma(m = 3) > \sigma(m = 2)$ above 500 K. This phenomenon was observed and elucidated by Melo Jorge et al. in terms of a semiconducting to metallic transition, induced by the doping level, defect distribution, and Mn valence state.[39]

To represent the total effects of the m value on the electrical behavior, we calculated the TE power factor (PF), which is defined as $PF = S^2\sigma$, for the different m values, with and without doping. The resulting PF values for the Nb-doped and undoped samples are displayed in Fig. 5a and b, respectively.

It is observed that the PF increases with increasing temperature for all samples. Moreover, the PF values of the Nb-doped RP phases systematically decrease with increasing CaO density, attaining the greatest values for $m = \infty$. We infer from this behavior that the property that mostly dominates the TE performance is the electrical conductivity. For the undoped samples, due to the relatively high intrinsic electrical conductivity of the $m = 3$ samples, the $m = 3$ and $m = \infty$ specimens exhibit a compensation effect with similar PF values.

There are only a few studies dealing with manganate-based RP phases in the TE context, however many deal with the role of substituent elements in the $m = \infty$ $CaMnO_3$ perovskite phase.[24–28,36,40–42] On the other hand, studies which deal with the TE properties of layered perovskite-type RP phases focus on $SrTiO_3$ (STO)-based oxides, that is, the $SrO(SrTiO_3)_n$ (n = integer) system.[18,19,43]

Wang et al.[19] and Lee et al.[18,43] found that the 5 at.% La- and Nb-doped $m = 1$ STO RP phase possesses lower PF than that of the $m = 2$ Nb-doped STO RP phase, by tens of $\mu W K^{-2} m^{-1}$, in accordance with our results. Furthermore, we note that the PFs reported by them for the STO RP phases are larger than those of our $CaMnO_3$ RP phases by approximately one order of magnitude.

Thermoelectric Figure of Merit

We calculated the *ZT* values for all the materials based on the measured electrical conductivity, Seebeck coefficient, and thermal conductivity, applying Eq. 2. The resulting *ZT* values of the Nb-doped and undoped samples are presented in Fig. 6a and b,

respectively. It can be seen that the ZT values of all the Nb-doped and undoped samples increase with increasing temperature up to 1000 K. This is a technologically important finding, indicating that improvement of the conversion efficiency of these materials is a question of thermal stability, in contrast to common TE compounds, for which the ZT values peak at lower temperatures. Furthermore, it is evident that, for Nb doping, the highest ZT value is obtained for the $m = \infty$ structure, with no CaO atomic layers, reaching ca. 0.1 at 1000 K. The lowest ZT value is obtained for $m = 1$ for both the Nb-doped and undoped materials, whereas for the other RP phases the ZT values range between those for $m = \infty$ and $m = 1$. An exception occurs for the undoped samples, as in the PF results, where $m = 3$ displays ZT values similar to those of $m = \infty$, which is related to its high intrinsic electrical conductivity values.

Comparison between the resulting ZT values of our manganate-based RP phases and those of the STO RP phases reveals that the latter possess higher ZT values,[18,19,43] by approximately one order of magnitude, for both $m = 1$ and 2 with Nb doping. Interestingly, for the STO RP system, the ZT value of the $m = 1$ structure is lower than that of the $m = 2$ one, in agreement with our results. We emphasize the important effects of the synthesis method on the resulting functional properties, including the TE figure of merit ZT; For instance, Bocher et al.[28] investigated the TE properties of $CaMnO_3$ with several Nb doping levels of 2 at.%, 5 at.%, and 8 at.% ($m = \infty$), synthesized using two different methods, namely "chimie douce" (SC) and the classical solid-state reaction (SSR). The SSR method reported by them is the most closely related to our processing method. Indeed, they report $ZT = 0.075$ at 1000 K for 5 at.% Nb doping, which is slightly lower than that achieved by us for similar conditions (4 at.% Nb), 0.095. The highest ZT values for both methods are obtained for 2 at.% doping, with a clear preference for the SC method (for all compositions), reaching the highest ZT value of 0.32.

CONCLUSIONS

Our study focuses on $CaO(CaMnO_3)_m$ n-type perovskites ($m = \infty$; 1 through 5), which are modulated structures formed of m perovskite $CaMnO_3$ layers separated by rock-salt CaO layers. We aim to draw a correlation between the TE properties of thermal conductivity, electrical conductivity, and thermopower and the periodicity of the planar defects, denoted by m, in these $CaO(CaMnO_3)_m$-based compounds. We prepared several pure and Nb-doped $CaO(CaMnO_3)_m$ compounds with different periodicities (m values) by mixing elemental powders and sintering at temperatures up to 1673 K. We performed basic materials characterization by XRD and HRSEM in combination with laser flash analysis for thermal conductivity measurements as well as electrical conductivity and thermopower measurements in the range from 300 K through 1000 K. Our main findings can be summarized as follows:

1. We managed to synthesize RP phases of the $CaO(CaMnO_3)_m$ form, either undoped or doped with 4 at.% Nb, having periodicities of $m = \infty$, 1, 2, and 3 for Nb doping. The rest ($m = 4^*$ and 5^* Nb-doped) were classified by us as mixtures of lower-m RP phases.
2. The $CaO/(CaMnO_3)_m$ multilayering configurations significantly reduce the thermal conductivity values compared with the $m = \infty$ base material; this was accompanied, however, by a reduction in the electrical conductivity and power factor, as well.
3. Nb substitution at Mn sublattice sites increased the electrical conductivity. In turn, the absolute values of the Seebeck coefficient decreased.
4. The differences in the electrical conductivity values of the RP phases decreased with increasing temperature, whereas the differences in the thermal conductivity values were retained up to 1000 K, having technological implications for high-temperature applications.
5. The greatest ZT values were obtained by us for $m = \infty$ at 1000 K, reaching 0.1 for Nb doping, which is typical for calcium manganate compounds. In spite of the desirable reduction of the thermal conductivity, the ZT values obtained for the RP phases are still low compared with those of the $m = \infty$ phases, possibly due to charge carrier scattering from the CaO layers.

In view of the above, there are several questions that remain open, involving issues such as dopant chemistry and concentration optimization, synthesis methods, and phase mixtures. Addressing these directions is expected to result in enhancement of the TE performance of calcium manganate compounds.

ACKNOWLEDGEMENTS

We deeply acknowledge Prof. Bertina Fisher, Dr. Larisa Patlagan, and Dr. Michael Reisner of the Physics Department, Technion, for helpful discussions. This research was carried out in the framework of the NEVET Program at the Nancy & Stephen Grand Technion Energy Program (GTEP), and supported by the Leona M. and Harry B. Helmsley Charitable Trust. Partial funding from the Russell-Berrie Nanotechnology Institute (RBNI) is acknowledged, as well. Generous support from the Israel Science Foundation (ISF), Grant No. 698/13, is gratefully acknowledged.

REFERENCES

1. D.M. Rowe, *Thermoelectrics Handbook: Macro to Nano* (Boca Raton: Taylor & Francis Group, 2006).

2. T.M. Tritt, *Annu. Rev. Mater. Res.* 41, 433 (2011).
3. G.J. Snyder and E.S. Toberer, *Nat. Mater.* 7, 105 (2008).
4. M. Zebarjadi, K. Esfarjani, M.S. Dresselhaus, Z.F. Ren, and G. Chen, *Energy Environ. Sci.* 5, 5147 (2012).
5. T.M. Tritt, *Thermal Conductivity: Theory, Properties, and Applications* (Clenson SC: Kluwer Academic/Plenum, Clemson University, 2004).
6. M. Ohtaki, *J. Ceram. Soc. Jpn.* 119, 770 (2011).
7. A. Weidenkaff, R. Robert, M. Aguirre, L. Bocher, T. Lippert, and S. Canulescu, *Renew. Energy* 33, 342 (2008).
8. S. Misture and D. Edwards, *Am. Ceram. Soc. Bull.* 91, 24 (2012).
9. K. Koumoto, Y. Wang, R. Zhang, A. Kosuga, and R. Funahashi, *Annu. Rev. Mater. Res.* 40, 363 (2010).
10. I. Terasaki, Y. Sasago, and K. Uchinokura, *Phys. Rev. B* 56, 12685 (1997).
11. A.C. Masset, C. Michel, A. Maignan, M. Hervieu, O. Toulemonde, F. Studer, B. Raveau, and J. Hejtmanek, *Phys. Rev. B* 62, 166 (2000).
12. J. He, Y.F. Liu, and R. Funahashi, *J. Mater. Res.* 26, 1762 (2011).
13. D.G. Cahill, P.V. Braun, G. Chen, D.R. Clarke, S. Fan, K.E. Goodson, P. Keblinski, W.P. King, G.D. Mahan, A. Majumdar, H.J. Maris, S.R. Phillpot, E. Pop, and L. Shi, *Appl. Phys. Rev.* 1, 011305 (2014).
14. S.M. Lee, D.G. Cahill, and R. Venkatasubramanian, *Appl. Phys. Lett.* 70, 2957 (1997).
15. W.S. Capinski, H.J. Maris, T. Ruf, M. Cardona, K. Ploog, and D.S. Katzer, *Phys. Rev. B* 59, 8105 (1999).
16. M.N. Touzelbaev, P. Zhou, R. Venkatasubramanian, and K.E. Goodson, *J. Appl. Phys.* 90, 763 (2001).
17. S.N. Ruddlesden and P. Popper, *Acta Crystallogr.* 11, 54 (1958).
18. K.H. Lee, S.W. Kim, H. Ohta, and K. Koumoto, *J. Appl. Phys.* 100, 7 (2006).
19. Y.F. Wang, K.H. Lee, H. Ohta, and K. Kournoto, *Ceram. Int.* 34, 849 (2008).
20. B. Fisher, L. Patlagan, G.M. Reisner, and A. Knizhnik, *Phys. Rev. B* 61, 470 (2000).
21. P. Ghosez and J.-M. Triscone, *Nat. Mater.* 10, 269 (2011).
22. H. Ohta, S. Kim, Y. Mune, T. Mizoguchi, K. Nomura, S. Ohta, T. Nomura, Y. Nakanishi, Y. Ikuhara, M. Hirano, H. Hosono, and K. Koumoto, *Nat. Mater.* 6, 129 (2007).
23. A. Graff and Y. Amouyal, *Appl. Phys. Lett.* 105, 181906 (2014).
24. M. Ohtaki, H. Koga, T. Tokunaga, K. Eguchi, and H. Arai, *J. Solid State Chem.* 120, 105 (1995).
25. G.J. Xu, R. Funahashi, Q.R. Pu, B. Liu, R.H. Tao, G.S. Wang, and Z.J. Ding, *Solid State Ionics* 171, 147 (2004).
26. D. Flahaut, T. Mihara, R. Funahashi, N. Nabeshima, K. Lee, H. Ohta, and K. Koumoto, *J. Appl. Phys.* 100, 4 (2006).
27. Y. Wang, Y. Sui, H.J. Fan, X.J. Wang, Y.T. Su, W.H. Su, and X.Y. Liu, *Chem. Mater.* 21, 4653 (2009).
28. L. Bocher, M.H. Aguirre, D. Logvinovich, A. Shkabko, R. Robert, M. Trottmann, and A. Weidenkaff, *Inorg. Chem.* 47, 8077 (2008).
29. J. de Boor, C. Stiewe, P. Ziolkowski, T. Dasgupta, G. Karpinski, E. Lenz, F. Edler, and E. Mueller, *J. Electron. Mater.* 42, 1711 (2013).
30. F. Edler and E. Lenz, *AIP Conf. Proc.* 1449, 369 (2012).
31. C. Cardoso, R.P. Borges, T. Gasche, and M. Godinho, *J. Phys. Condens. Matter* 20, 035202 (2008).
32. C. Autret, C. Martin, M. Hervieu, R. Retoux, B. Raveau, G. Andre, and F. Bouree, *J. Solid State Chem.* 177, 2044 (2004).
33. I.D. Fawcett, J.E. Sunstrom, M. Greenblatt, M. Croft, and K.V. Ramanujachary, *Chem. Mater.* 10, 3643 (1998).
34. M.E. Leonowicz, K.R. Poeppelmeier, and J.M. Longo, *J. Solid State Chem.* 59, 71 (1985).
35. J. Takahashi and N. Kamegashira, *Mater. Res. Bull.* 28, 565 (1993).
36. L. Bocher, M.H. Aguirre, R. Robert, D. Logvinovich, S. Bakardjieva, J. Hejtmanek, and A. Weidenkaff, *Acta Mater.* 57, 5667 (2009).
37. B. Raveau, Y.M. Zhao, C. Martin, M. Hervieu, and A. Maignan, *J. Solid State Chem.* 149, 203 (2000).
38. C. Kittel, *Introduction to Solid State Physics*, 6th ed. (New York: Wiley, 1986).
39. M.E. Melo Jorge, M.R. Nunes, R.S. Maria, and D. Sousa, *Chem. Mater.* 17, 2069 (2005).
40. J.L. Lan, Y.H. Lin, A. Mei, C.W. Nan, Y. Liu, B.P. Zhang, and J.F. Li, *J. Mater. Sci. Technol.* 25, 535 (2009).
41. A. Kosuga, Y. Isse, Y.F. Wang, K. Koumoto, and R. Funahashi, *J. Appl. Phys.* 105, 6 (2009).
42. L. Bocher, R. Robert, M.H. Aguirre, S. Malo, S. Hebert, A. Maignan, and A. Weidenkaff, *Solid State Sci.* 10, 496 (2008).
43. K.H. Lee, Y.F. Wang, S.W. Kim, H. Ohta, and K. Koumoto, *Int. J. Appl. Ceram. Technol.* 4, 326 (2007).